

DOI: 10.1002/adem.201180057

## Structure and Mechanical Performance of a “Modern” Fish Scale\*\*

By Deju Zhu, Cesar Fuentes Ortega, Ramak Motamedi,  
Lawrence Szewciw, Franck Vernerey and Francois Barthelat\*

*Protective materials and structures found in natural organisms may inspire new armors with improved resistance to penetration, flexibility, light weight, and other interesting properties such as transparency and breathability. All these attributes can be found in teleost fish scales, which are the most common types of scales in modern fish species. In this work, we have studied the structure and mechanics of fish scales from striped bass (*Morone saxatilis*). This scale is about 200–300  $\mu\text{m}$  thick and consists of a hard outer bony layer supported by a softer cross-ply of collagen fibrils. Perforation tests with a sharp needle indicated that a single fish scale provides a high resistance to penetration which is superior to polystyrene and polycarbonate, two engineering polymers that are typically used for light transparent packaging or protective equipment. Under puncture, the scale undergoes a sequence of two distinct failure events: First, the outer bony layer cracks following a well defined cross-like pattern which generates four “flaps” of bony material. The deflection of the flaps by the needle is resisted by the collagen layer, which in biaxial tension acts as a retaining membrane. Remarkably this second stage of the penetration process is highly stable, so that an additional 50% penetration force is required to eventually puncture the collagen layer. The combination of a hard layer that can fail in a controlled fashion with a soft and extensible backing layer is the key to the resistance to penetration of individual scales.*

Nature increasingly serves as a model and inspiration to scientists and engineers, and biomimetics has the potential to lead to novel engineering materials and systems with new combinations of properties, multi-functionalities, adaptability, and environmental sustainability. In this work, we have studied the structure and mechanics of modern teleost fish scales, which have received relatively little attention in the

past.<sup>[1–5]</sup> This type of scale displays interesting combinations of flexibility, strength, resistance to penetration, light weight, and transparency. Fish scales exhibit large variations in shape, size, and arrangement. The general classification includes cosmoid, ganoid, placoid, and elasmoid (cycloid and ctenoid) found in the modern teleost class of fishes.<sup>[6]</sup> The “primitive” cosmoid and ganoid scales are bulky, bony scales which offer very effective protective properties, through a multilayered structure capable of a variety of dissipative mechanisms.<sup>[3]</sup> However, over the course of evolution the reduction of the integumental skeleton has improved swimming performance,<sup>[3,7]</sup> and the “ancient” cosmoid and ganoid scales have been replaced by the thinner, more flexible teleost scales.<sup>[8]</sup> Teleost scales have excellent hydrodynamic properties<sup>[9,10]</sup> and provide a protective layer resisting penetration.<sup>[3,7,8]</sup> Currey, in a review article on mineralized tissues, noted that some fish scales are so tough that they cannot be easily fractured even after immersion in liquid nitrogen.<sup>[11]</sup> At larger lengths, the arrangement of the scales provides a flexible skin that allows for changes in shape. In fact, the scaled skin has been shown to play a critical structural role in fish locomotion by regulating wave propagation<sup>[12–14]</sup> and by storing mechanical energy in order to make swimming more efficient.<sup>[15]</sup>

[\*] Dr. D. Zhu, C. F. Ortega, R. Motamedi, L. Szewciw,  
Dr. F. Barthelat  
Department of Mechanical Engineering,  
McGill University, Montreal, QC, (Canada)  
E-mail: francois.barthelat@mcgill.ca  
Dr. F. Vernerey  
Department of Civil Engineering,  
University of Colorado, Boulder, CO, (USA)

[\*\*] The authors wish to acknowledge the support of the National Science Foundation under award CMMI 0927585 and of Faculty of Engineering at McGill University. Atomic emission spectroscopy tests were performed by Monique Riendeau, Dept. of Mining & Materials Engineering, and Ranjan Roy and Andrew Golsztajn, Dept. of Chemical Engineering, McGill University.

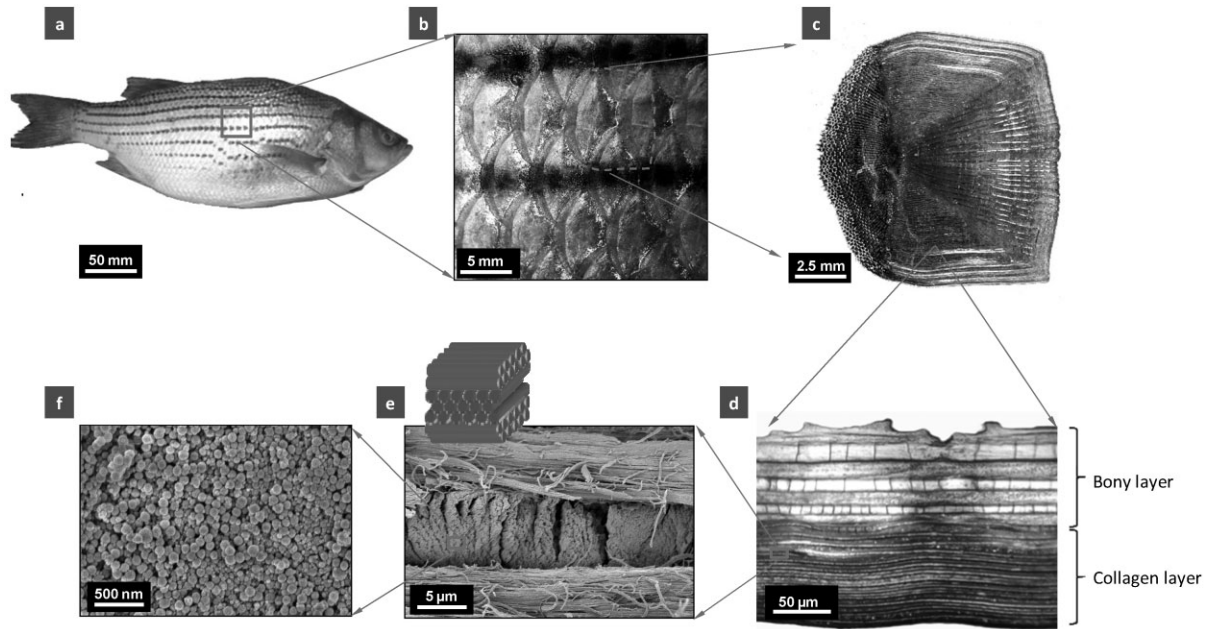


Fig. 1. The hierarchical structure of a teleost fish scale from striped bass, *M. saxatilis*. (a) Whole fish, (b) staggered multiple scales, (c) an individual scale, (d) cross-section of a scale, (e) cross-ply collagen structure, (f) collagen fibrils.

### 1. The Hierarchical Structure of Fish Skin

In this study we have investigated the structure and mechanics of a single teleost (ctenoid) fish scale from striped bass *Morone saxatilis*. Like many other structural biological materials,<sup>[16–18]</sup> the structure of teleost fish scales displays a characteristic hierarchical structure, built over several distinct length scales (Figure 1). At the macroscopic level, the scales are staggered and cover most of the body of the fish (Figure 1a,b). This arrangement provides a continuous barrier to penetration and flexural compliance. When the fish is highly curved (at the end of a swimming stroke), the scales interact more strongly, which stiffens the skin in flexion.<sup>[19]</sup> The skin then acts as an “external tendon,” storing mechanical energy, which can be recovered to facilitate the onset of the next stroke.<sup>[15,20]</sup> At the mesoscale level, an individual scale from an adult striped bass is a thin plate with an irregular pentagonal shape, about 10 mm in diameter (Figure 1c).

The posterior area of the scale displays rough patterns (ctenii) which offer attractive hydrodynamic properties,<sup>[9,10]</sup> while the anterior area consists of grooves in the radial direction (radii) and ridges that form circular rings (circuli) around a central area called the “focus.”<sup>[21]</sup> Radii and circuli possibly provide increased flexibility and anchoring of the scale, respectively.<sup>[10]</sup> Teleost scales are composed of collagen fibrils type-I, and are partially mineralized with hydroxyapatite (16–59% mineral content in weight<sup>[2,5,22–24]</sup>). The outer layer of the scale is significantly more mineralized and often referred to as “bony layer,” whereas the inner layer (“basal” or “collagen” layer) is mineralized mostly near the bony layer, but with mineralization pockets proceeding well into the collagen layer.<sup>[7,23]</sup> In striped bass, bony and collagen layers have approximately the same thickness (100 μm). Using AES

(atomic emission spectroscopy), we measured an average hydroxyapatite mass fraction of 46% for the whole scale. The density of collagen ( $1.33 \times 10^3 \text{ kg} \cdot \text{m}^{-3}$ ) and hydroxyapatite ( $3.17 \times 10^3 \text{ kg} \cdot \text{m}^{-3}$ )<sup>[21]</sup> were used to estimate the volume fraction of hydroxyapatite as 26%. In another experiment, we separated a scale into two samples by dissecting a few plies off the collagen layer. The upper and lower samples gave hydroxyapatite mass contents of 50% and 14%, respectively (30% and 6% in volume fractions), confirming that the upper region of the scale is significantly more mineralized than the lower region. These results are consistent with reports of a general 20–35% percentage points difference in mineralization between the bony and collagen layers.<sup>[25]</sup> Bony and collagen layers are cross-ply layered composites, each ply being made of parallel collagen fibrils rotated across layers by angles that can vary from species to species.<sup>[25–29]</sup> In striped bass, we found that the basal layer is formed of 20–25 plies about 4–5 μm thick each (Figure 1d), where the collagen fibrils are rotated by 90 degrees from one ply to the next (Figure 1e). Cross-ply collagen structures are typically found in natural tissues that undergo multiaxial stresses (shell of soft-shelled turtles,<sup>[30]</sup> human annulus fibrosus<sup>[31]</sup>). Several authors have discussed the importance of the plywood nature of the collagen layer to whole fish scale mechanical properties,<sup>[2,5,8,32–34]</sup> in general by providing the scale with strength along multiple directions. At smaller length scales, individual collagen fibrils, about 50–200 nm in diameter, can be observed on a cross-section of the scale (Figure 1f). Interestingly, we found that in striped bass the 90 degree cross-ply is achieved by alternating layers composed of radial fibrils (“R” layers) with layers made of circumferential fibrils (“C” layers), both layers being organized around the focus of the scale (Figure 2). This arrangement is consistent with the growth of individual

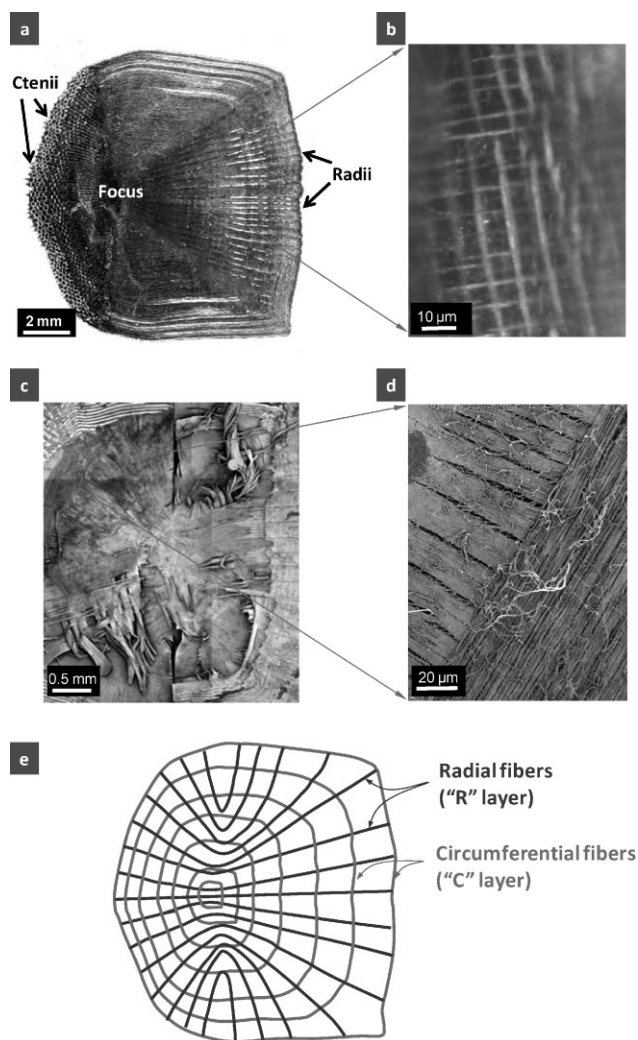


Fig. 2. Arrangement of the collagen fibrils in a striped bass scale. (a) Top view of the whole scale showing surface features (optical micrograph); (b) bottom view showing collagen fibers in the collagen layer; (c) removal of the bony layer reveals the radial-circumferential (R-C) pattern of the collagen fibrils; (d) locally, the fibers are orthogonal from one layer to the next; (e) schematics of the R-C pattern.

scales, which occurs by deposition of collagen at the periphery of the scale.<sup>[35,36]</sup>

## 2. Tensile Testing on Individual Scales

In order to assess the mechanical response of individual scales, we performed tensile tests in hydrated conditions on small tensile samples prepared from individual scales. Whole, fresh striped bass (*Morone saxatilis*) were acquired from a fish supplier (Nature's Catch, Inc., Clarksdale, MS, USA) and kept on ice. Scales were plucked using tweezers and stored in a freezer at  $-20^{\circ}\text{C}$  until tested. Before the test, the scales were removed from the freezer and put in a water bath for about 5 min for thawing, and then cut into small dog-bone-shaped specimens using a multi-tube rotary hole-punch and dissecting scissors. The resulting samples had a gage length of 4 mm, a gage width of 1.5 mm and an average thickness of about

0.20 mm. Using this technique, samples were cut at 0, 45, and  $90^{\circ}$  from the longitudinal direction (anteroposterior axis) of the fish.

The samples were then mounted on a miniature loading stage (Ernest F. Fullam Inc., Latham, NY), which was placed under an upright, reflected light microscope (BX-51M, Olympus, Markham, Canada) equipped with a CCD camera (RETIGA 2000R, Qimaging, Surrey, Canada) in order to monitor deformations and failure modes of the specimens. All specimens were loaded in tension at a rate of  $0.005\text{ mm}\cdot\text{s}^{-1}$  (corresponding to a strain rate of  $1.25\times 10^{-3}\text{ s}^{-1}$ ) up to complete failure. Images were taken throughout the entire test every 10 s using the CCD camera. The images were used to measure the deformation and strain values of the samples using digital image correlation<sup>[37]</sup> and to monitor failure modes such as debonding of the bony layer and pullout of the collagen fibrils. All samples were kept in hydrated conditions during preparation and testing.

The resulting stress-strain curves (Figure 3a) display an initial quasi-linear region, with an initial modulus in the 600–850 MPa range. The material softens slightly before reaching a maximum stress of 30–50 MPa (depending on scale orientation), after which the stress drops significantly. Using optical observation, we could associate this sudden decrease in stress to the sudden cracking of the bony layer. Subsequently, the collagen layer progressively detaches from the stiff bony layer, while collagen plies tear one after the other, yielding step-like patterns on the stress-strain curve up to total failure at about 40% strain.

In order to assess the mechanical response of the collagen layer alone, we performed additional tensile tests on scales with the bony layer removed. The collagen layer was carefully peeled out of the scale which rested on a flat and hard surface. The layered structure of the fish scale makes it easy to "delaminate" with a minimum of force. While the collagen material at the separation site might be partially damaged, the peeling force was deemed insufficient to damage the rest of the collagen layer and to alter its overall mechanical properties. The remaining 0.05 mm thick collagenous material was tested in tension along the 0, 45, and  $90^{\circ}$  directions.

The stress-strain response (Figure 3a) displayed a linear regime with a modulus of about 450 MPa, followed by a progressive failure after a peak stress of 65 MPa. The ultimate strain was the same with and without bony layer. The behavior of the collagen cross-ply is consistent with the behavior of single collagen type I fibrils.<sup>[38]</sup> Assuming that the fibers do not carry any stress if they are perpendicular to the loading direction, only half of the material actually carries stress in the collagen layer. Since individual collagen fibrils have a Young's modulus of about 1 GPa, a tensile strength of 200 MPa and a strain at failure of 30%,<sup>[38]</sup> the modulus of the  $90^{\circ}$  ply laminate can be estimated at 500 MPa, its strength at 100 MPa and its strain at failure at 30%. This compares well with our experimental results, showing that the tensile behavior of the collagen layer is largely controlled by the stretching of straight, individual collagen fibrils.

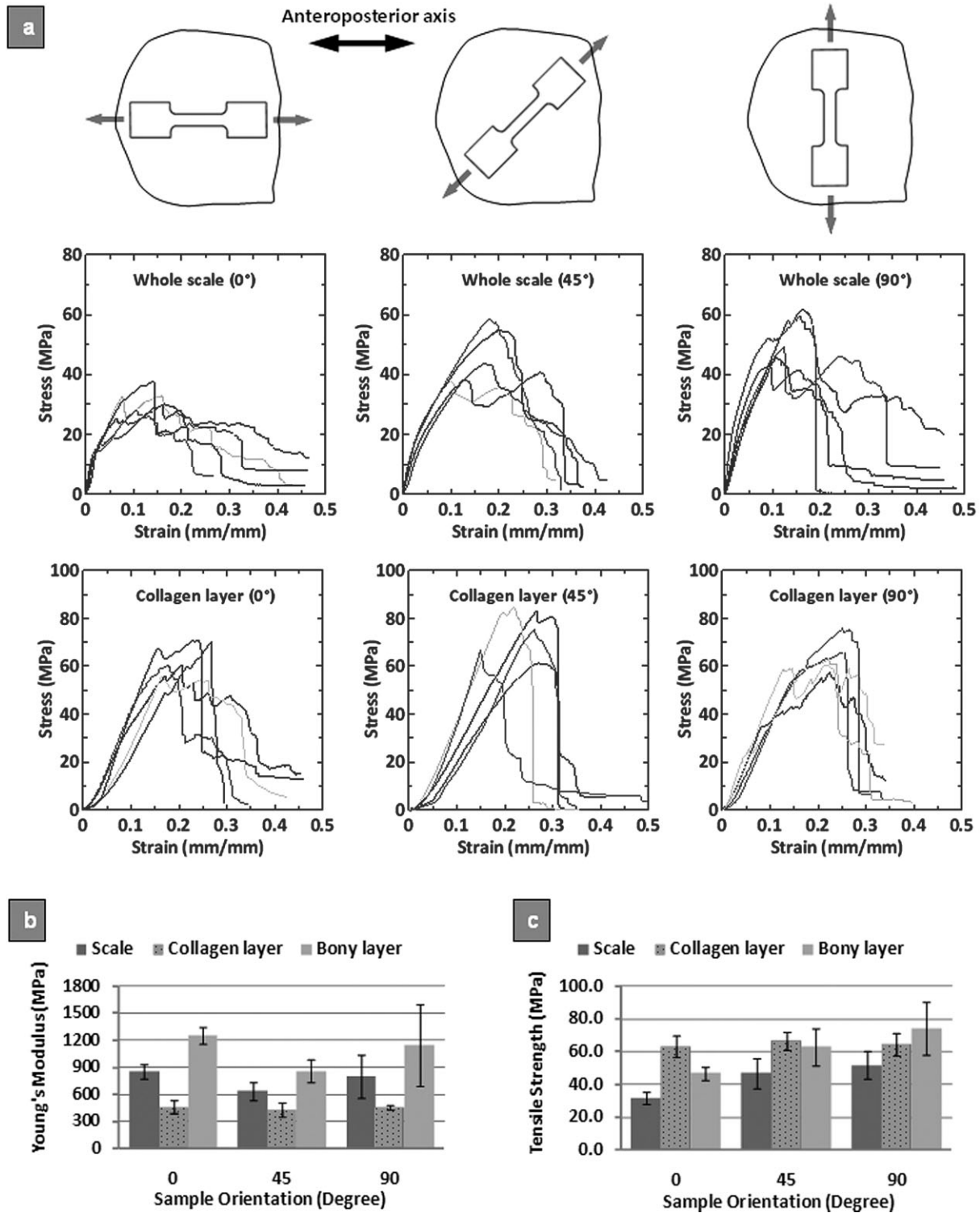


Fig. 3. (a) Tensile stress–strain curves for fish scales along 0, 45, and 90° from the longitudinal axis of the fish. Summary of results for (b) Young's modulus; (c) strength. The error bars indicate standard deviations.

While it was not possible to isolate the bony layer for testing, its properties were inferred from the whole scale and collagen only tensile test results. In the elastic regime, the whole scale behaves like a two-layer, constant strain composite. Since the thickness of the bony and collagen layers is similar, the modulus of the scale is

given by:

$$E_S = \frac{1}{2}(E_C + E_B) \quad (1)$$

where  $E_C$  and  $E_B$  are the Young's moduli of collagen and bony layers, respectively. The modulus of bony layer can then be

estimated using:

$$E_B = 2E_S - E_C \quad (2)$$

The strength of bony layer can be evaluated with a similar approach. In the linear regime, with the uniform strain assumption, the stresses in the bony and collagen layers are proportional to their stiffnesses. From the whole scale test, the stress  $\sigma_S$  at which the bony layer fails is known. Just prior to failure the stress in the bony layer is then given by:

$$\sigma_B = \frac{E_B}{E_S} \sigma_S \quad (3)$$

This model assumes that both materials are in the linear elastic range up to the failure of the bony layer. In reality Figure 3a shows that the scale softens slightly when loaded in tension, probably due to damage accumulation in the bony layer (collagen behaves linearly over this range of strain). Equation 3 therefore slightly overestimates the actual strength of the bony layer. We used Equations (2) and (3) to estimate the modulus and strength of the bony layer. The results show that the bony layer is about twice as stiff as the collagen layer, with about the same tensile strength (Figure 3b,c). The bony layer is, however, more brittle, failing at about 10% strain while the collagen layer fails at strains in excess of 40%. Interestingly, we also found that the whole scale displays in-plane anisotropic properties, but only because of the bony layer; the collagen layer is isotropic in plane in terms of both modulus and strength. This set of experiments highlights the main traits of the scale's components: the bony layer is stiff, hard and brittle because of its high mineral content, while the underlying collagen cross-ply is softer and more deformable, with larger strains at failure.

### 3. Resistance to Sharp Penetration: Puncture of Individual Scales

Adult striped bass have a few natural predators, including various aquatic birds, marine mammals, and potentially large

pelagic fishes and sharks.<sup>[39]</sup> Juveniles striped bass are known to have several sources of predation including bluefish (*Pomatomus saltatrix*) and cannibalism.<sup>[39]</sup> The main function of the scales is mechanical protection against predators<sup>[3,7,8]</sup> and, in particular, the scale must be capable of preventing sharp objects such as teeth<sup>[40]</sup> from completely penetrating the skin and reaching the softer and more fragile underlying tissues. A sharp tooth concentrates the biting force over a very small area on the scale, which leads to severe contact stresses. We have assessed the resistance to penetration of single striped bass scales using an experimental setup that simulates a predator's bite using the same miniature loading stage described above in the tensile tests. A sharp steel needle (tip radius = 25  $\mu\text{m}$ ) was used to simulate a predator's tooth (bluefish, for example, have teeth of a shape similar to a needle and a radius smaller than 250  $\mu\text{m}$ ). The needle was driven through a scale resting on a silicone rubber substrate ( $E \approx 1.8 \text{ MPa}$  measured by spherical indentation) used to simulate the soft dermis and tissues underlying the scale, at a speed of  $0.005 \text{ mm} \cdot \text{s}^{-1}$  while the force was recorded (Figure 4a). The load-deflection curves resulting from these tests were highly repeatable throughout all tested samples, with a slight force drop at about 2 N and a maximum penetration force of 3–3.5 N (Figure 4b). For comparison, we also performed puncture tests on thin polystyrene (PS) and polycarbonate (PC), which are modern engineering polymers typically used when light weight, stiffness, strength, optical translucence, and impact resistance are required (their applications include CD cases, biomedical equipment such as petri dishes, and protective gear such as safety glasses or squash goggles). For proper comparison we prepared 10 mm diameter disks of these polymers, and we adjusted the thickness so the areal density (the mass per unit area of protective material) of the protective layer was then same for fish scale, PC and PS. Remarkably, the fish scale provided a significantly higher resistance to puncture compared to these high performance engineering polymers (Figure 4b).

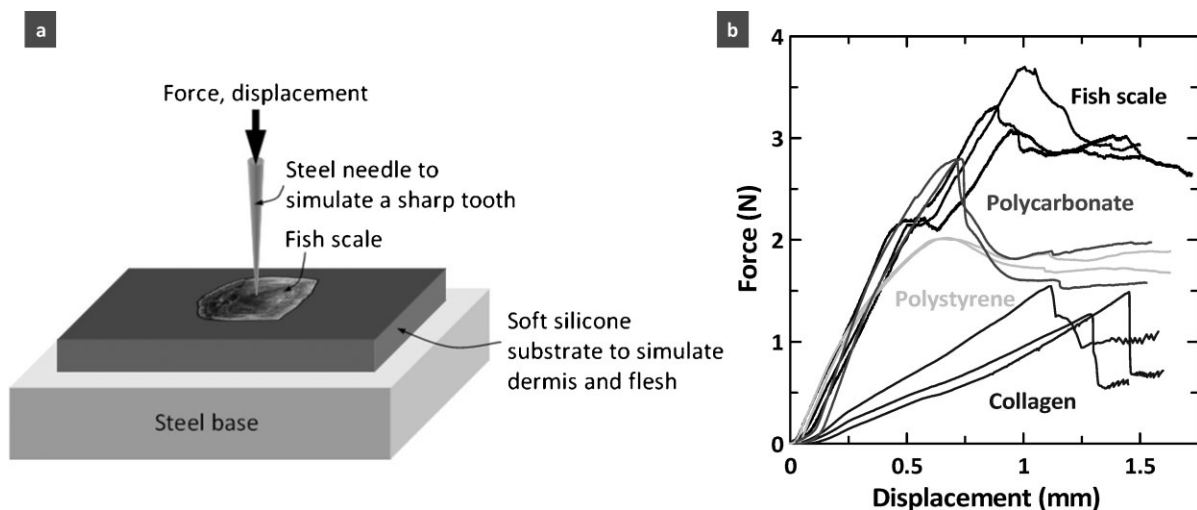


Fig. 4. (a) Experimental setup for the puncture test; (b) typical results for striped bass scales with and without bony layer. Results for polystyrene and polycarbonate are also shown for comparison.

Finally, we performed additional puncture tests on scales with the bony layer removed. The isolated collagen layer was easily penetrated, providing only half of puncture resistance in terms of force. The bony layer is therefore an important component of the system, operating in synergy with the collagen layer to increase the performance of individual scales. The fish scale followed a sequence of mechanisms that was highly repeatable from scale to scale as well as across locations on a given scale. The penetration curves consist of three distinct stages that we investigated in detail by imaging of the puncture site at different points on the penetration curve (Figure 5). Stage I is the initial linear region, which is dominated by flexion of the entire scale and by damage and indentation of the surface of the bony layer. At a force of about 2 N, the force drops slightly, which we associated to the sudden cracking of the bony layer. Bony and collagen layers

have the same thickness, but since the bony layer is stiffer, the neutral plane of the scale lies within the bony layer. As a result, flexural deformations generate tensile stresses in the lower side of the bony layer. Once these stresses reach the tensile strength of the bony layer, cracks initiate at the collagen/bone interface and rapidly propagate towards the surface of the bony layer. Interestingly, the patterns of the flexural cracks always followed a cross pattern, whose orientation invariably followed the orientation of the local radii and circuli (Figure 5c) and underlying collagen fibrils. The microstructure of the bony layer therefore induces the failure of the bony layer along specific directions. Upon cracking of the bony layer, four "flaps" of bony material immediately deflect downwards, generating circumferential cracks. At this point, the underlying collagen layer, while remaining intact, detaches from the bony layer over a ring-like

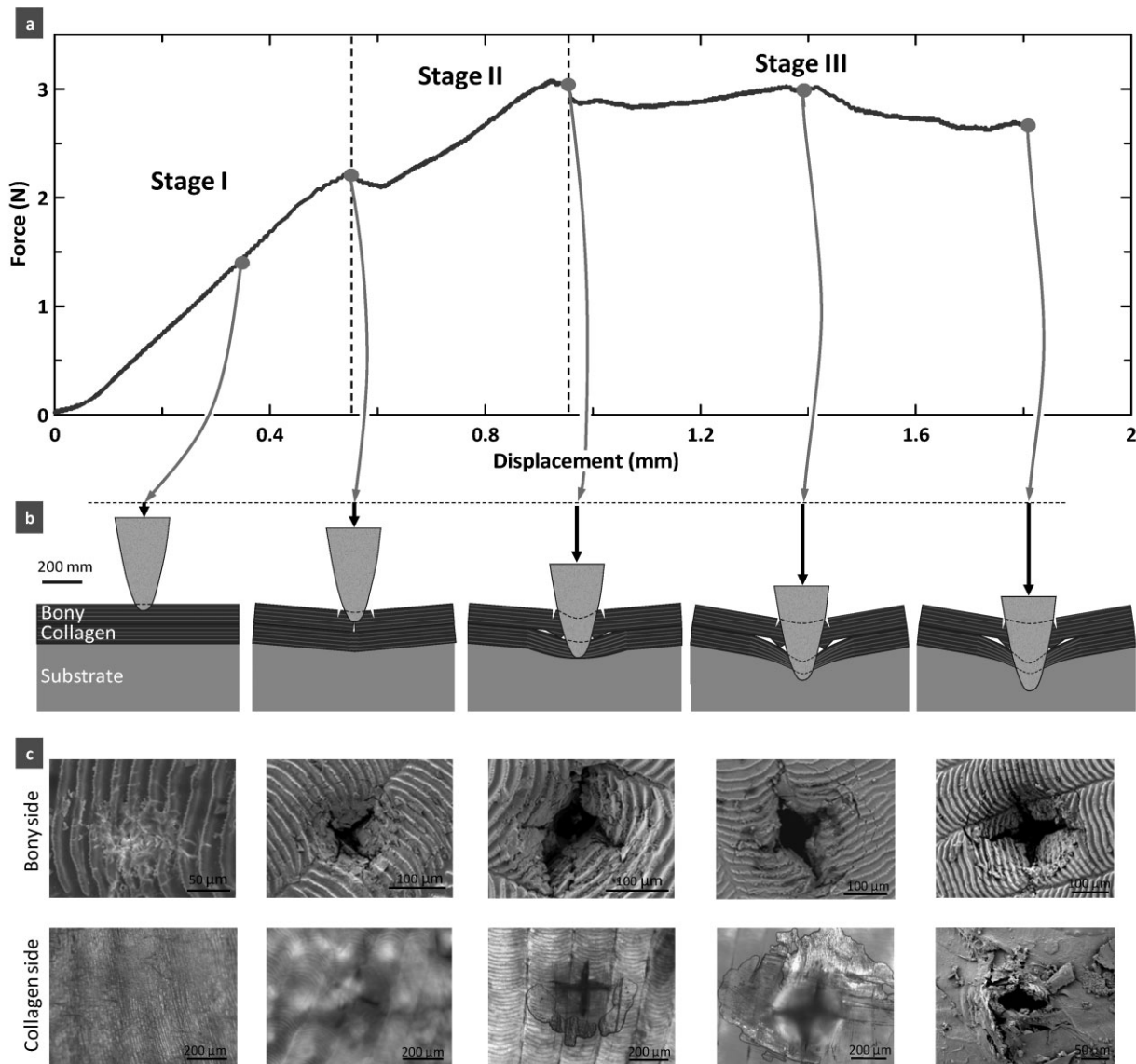


Fig. 5. Detailed sequence of a puncture test. (a) Load–displacement curve showing three distinct stages; (b) associated mechanisms; and (c) imaging. The images of the bony side and the last one of the collagen side were obtained by scanning electron microscopy (SEM), while the first four images of the collagen side were taken with an optical microscope.

area observable with an optical microscope (the scale, while opaque to electrons, is transparent to visible light). The cracking of the bony layer marks the beginning of stage II, dominated by further flexion of the scale, opening of the cross cracks as the four "flaps" of bony material are bent towards the collagen layer, radial propagation of the cross cracks, and further delamination between collagen and bony layers. Eventually the deflection and opening of the flaps are sufficient to let the needle reach the collagen layer and completely puncture it (stage III). The initial failure of the collagen layer indicates the beginning of stage III, and the sharp drop in force at this point suggests that the failure is rapid, possibly because the collagen layer is stretched. Throughout the rest of stage III, the scale is deflected by the needle, the delamination between collagen and bony layers propagates more extensively, and the radial cracks continue to grow.

We further investigated the mechanisms operating at stage II, since they are powerful enough to increase the resistance of the scale by an additional 1 N (representing an additional 50% of the load at failure of the bony layer). In particular, we examined the controlled deflection of the four "bony flaps" using an idealized three-dimensional geometry shown in

Figure 6a,b. Each of the four flaps was assumed to be rigid and hinged along a straight line at the bone/collagen interface. The force from the needle was assumed to be evenly distributed between the tips of the 4 flaps. Only two mechanical loads resist the deflection of the flaps by balancing the force from the needle: i) the bending moment transmitted through the remaining ligament of the bony layer, and ii) the intact collagen layer, which acts as a "retaining membrane" for the flaps. Interestingly, in this configuration the collagen layer is in a state of biaxial tension at the penetration site, and the purpose and advantage of its cross-ply structure becomes evident.

The bending moment transmitted at the ligament was evaluated by assuming perfect plasticity in the bony layer with  $\sigma_Y = 60$  MPa (evaluated from our tensile test). In order to balance this moment, the force applied by the needle was estimated at 1.2 N (see Appendix for calculation details), which is actually below the force at which the bony layer fractures. This value represents an upper bound estimate, since in reality the bony layer probably cracks before the full plastic state can be reached. This prediction shows that in stage II, there is no bending moment transmitted at the bony flaps, and that the flaps can be assumed to rotate about

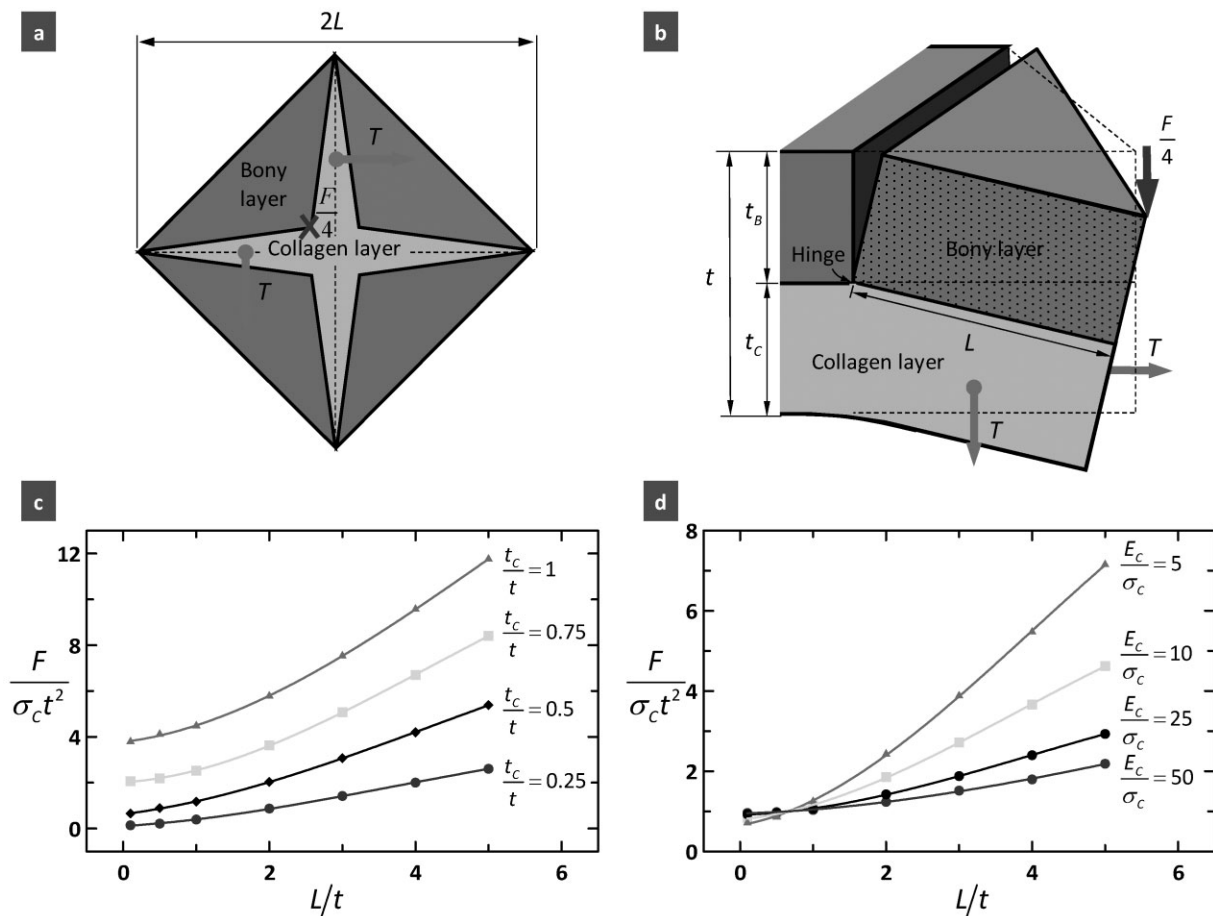


Fig. 6. (a) Top view of the idealized puncture configuration; (b) three-dimensional view of single bony flaps. The force applied by the needle ( $F/4$ ) and the forces generated by the tension in the collagen layer are shown. (c) Effect of collagen layer thickness and (d) collagen resilience on the normalized penetration force.

frictionless hinges. The experiments show circumferential cracks in the region of the hinges, confirming that little or no bending moment can be transmitted through the bony hinge. The second mechanism examined was associated with the collagen, which acts as a retaining membrane for the flaps.

In the model, the collagen layer was assumed to have completely delaminated from the overlying surface of the bony layer, which is consistent with experimental observations towards the end of stage II. The collagen layer then acts as a retaining membrane, with biaxial tension as the dominant stress. Based on the idealized geometry, the moment balance of a single bony flap about the hinge led to a simple expression for the penetration force as a function of bony and collagen layer thickness ( $t_B, t_C$ ), length of the flaps ( $L$ ), and stiffness ( $E_C$ ) and strength ( $\sigma_C$ ) of the collagen layer. Full penetration at the end of stage II was assumed to be reached when the collagen failed in tension (at a stress of 65 MPa according to our tensile tests). Our model predicted a penetration force of  $F = 3N$  based on the properties of the collagen layer ( $E_C = 500$  MPa,  $\sigma_C = 65$  MPa) and optical observation ( $t_B = t_C = 100 \mu\text{m}$ ,  $L = 200 \mu\text{m}$ ). This prediction is remarkably close to penetration force we measured experimentally, which demonstrates that the retaining membrane effect dominates stage II and controls the ultimate penetration resistance of the scale.

In terms of design, the model reveals that longer flaps are desirable, and since  $L$  is larger for larger "teeth" and higher forces, the scale provides a greater resistance to penetration for larger teeth and stronger bites (Figure 6c,d). A thick collagen layer is also beneficial, although a minimum of bony material is required to form stiff flaps. This finding substantiates previous discussions on mechanical benefits of thicker collagen fibrils and plywood organization in the collagen layer.<sup>[8,32,33,41]</sup> Finally, a soft and strong material increases resistance to penetration, although a too soft backing layer may lead to excessive deflection that may damage the underlying tissues even before needle penetration. A cross-ply of collagen is therefore ideal for this function, and the function of the harder bony layer is to protect the collagen layer from direct contact with the tip of the needle, and to mitigate the stresses transmitted onto the softer collagen layer by redistributing them over a large area.

**4. Conclusions**

Individual teleost fish scales are therefore high performance natural protective systems, offering resistance to puncture superior to modern engineering polymers typically used for protective applications. Remarkably, fish scales are made of a set of materials that are both softer and weaker than these engineering polymers, which highlights the important role of the structure and architecture of the scale in "amplifying" the properties (as seen in other class of biological materials<sup>[42-44]</sup>). The high performance of the scales is the result of a fine balance of structure and material properties, and in particular the hardness and stiffness of the outer layer, the softness and strength of the inner layer, and an

interface weak enough to delaminate and allow the collagen layer to stretch under the bony flaps. While this first study on the puncture mechanics of fish scale does not consider viscous effects, it is likely that viscoelastic and viscoplastic effects also contribute to the energy dissipation capability of the scale. The actual skin of the fish is of course covered with a large number of overlapping scales and, for striped bass, we counted that any given point on the surface of the body is covered with 3 or 4 layers of scales. The resulting multilayer system alternates hard and soft layers in an arrangement reminiscent of the design of bulletproof glass. In addition, overlapping scales ensures compliance and breathability, two highly desirable properties for personal armors. A biomimetic design at the individual scale level could therefore be combined with a clever arrangement of the scales at the macroscale to yield a hierarchical protective system with attractive properties.

*Appendix: Analytical "Four Flaps" Model*

A simplified analytical model was derived to capture the progressive deflection of the four flaps and the retaining membrane effect provided by the underlying collagen layer (Figure A.1).

*A.1. Strain*

The strains in the collagen were determined by tracking the displacement of the point in the centroid of the section of collagen (point D). Upon deflection of the flap point D moves to D', so that its displacement vector can be written, in the Cartesian system  $xyz$  (Figure A.1):

$$DD' = \begin{bmatrix} \frac{L}{2\sqrt{2}}(\cos\theta - 1) - \frac{t_C}{2}\sin\theta \\ 0 \\ -\frac{L}{2\sqrt{2}}\sin\theta - \frac{t_C}{2}(\cos\theta - 1) \end{bmatrix} \tag{A.1}$$

Any fiber crossing the cracks will extend by a distance (using scalar product to project  $DD'$  on the unit vector collinear to  $T$ ):

$$\begin{bmatrix} \frac{L}{2\sqrt{2}}(\cos\theta - 1) - \frac{t_C}{2}\sin\theta \\ 0 \\ -\frac{L}{2\sqrt{2}}\sin\theta - \frac{t_C}{2}(\cos\theta - 1) \end{bmatrix} \cdot \begin{bmatrix} -\frac{1}{\sqrt{2}} \\ \frac{1}{\sqrt{2}} \\ 0 \end{bmatrix} = \frac{L}{4}(1 - \cos\theta) + \frac{t_C}{2\sqrt{2}}\sin\theta \tag{A.2}$$

The collagen is detached from the bony layer in the puncture area, which leads to the assumption that the tensile strain in the collagen is uniform and equal to:

$$\epsilon_C = \frac{1}{2}(1 - \cos\theta) + \frac{t_C}{L\sqrt{2}}\sin\theta \tag{A.3}$$

Interestingly, the geometry and kinematics for the system is such that the strain in the collagen layer is equi-biaxial and uniform in the puncture site. Knowledge of strain in the collagen layer leads to stress, using the modulus found from the tensile tests ( $E = 500$  MPa).

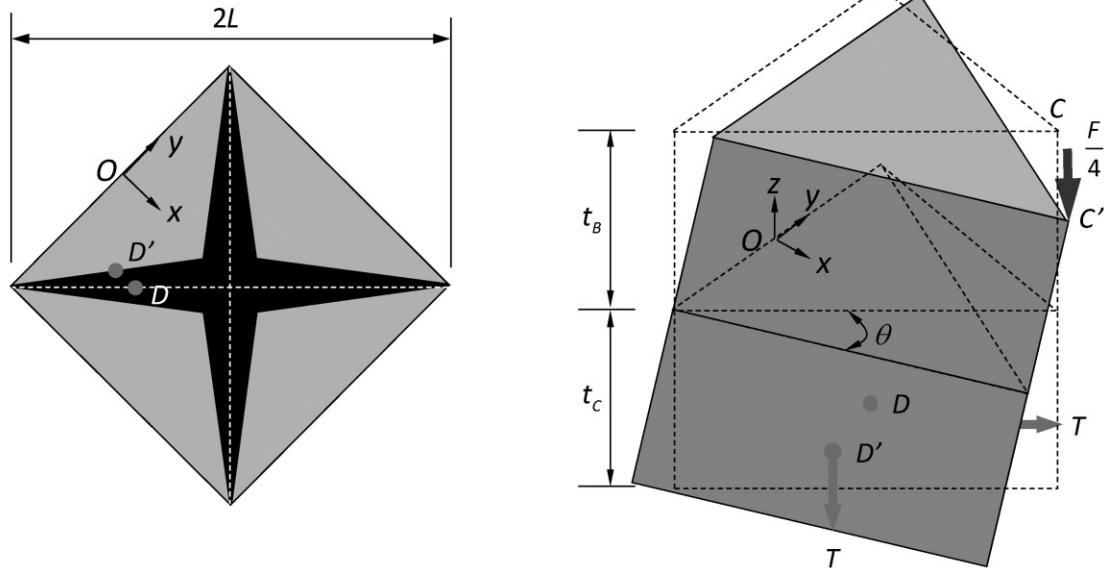


Fig. A.1. Schematic diagram of the deformation and force in the four flaps model.

A.2. Deflection of the Flaps

Similarly, point C at the upper tip of the flaps moves to C' upon deflection, and

$$CC' = \begin{pmatrix} \frac{L}{\sqrt{2}}(\cos\theta - 1) + t_B \sin\theta \\ 0 \\ -\frac{L}{\sqrt{2}}\sin\theta + t_B(\cos\theta - 1) \end{pmatrix} \quad (A.4)$$

The deflection at the loading point is then the z component of CC':

$$\delta = \frac{L}{\sqrt{2}}\sin\theta - t_B(\cos\theta - 1) \quad (A.5)$$

A.3. Force

Under the concentrated force F/4, the rigid bony flap rotates along the y axis and the loading location changes from C to C'. The force vectors acting on the bony and collagen layers are:

$$\vec{F} = \begin{bmatrix} 0 \\ 0 \\ -F/4 \end{bmatrix} \quad \vec{T} = \begin{bmatrix} \frac{T}{\sqrt{2}} \\ \frac{T}{\sqrt{2}} \\ 0 \end{bmatrix} \quad (A.6)$$

As the cross product of the vectors OD' and T is equivalent to half of the cross product of the vectors OC' and F, then we

get the force retained by the collagen layer as follows:

$$F = 2Lt_C\sigma_C \left( \frac{\sqrt{2}\tan\theta + 2\frac{t_C}{L}}{1 + \sqrt{2}\frac{t_B}{L}\tan\theta} \right) \quad (A.7)$$

Normalized by the square of the scale thickness t and the tensile strength of collagen sigma\_C:

$$\frac{F}{\sigma_C t^2} = 2\frac{L}{t} \frac{t_C}{t} \left( \frac{\sqrt{2}\tan\theta + 2\frac{t_C}{L}}{1 + \sqrt{2}\frac{t_B}{L}\tan\theta} \right) \quad (A.8)$$

A.4. Force Generated by Flexural Stresses at the Hinges

Assuming that the entire thickness of the bony layer undergoes plasticity, the bending moment transmitted is calculated as follows:

$$M = \sqrt{2}L \left( \frac{t_B}{2} \right)^2 \sigma_B \quad (A.9)$$

The force applied by the needle is balanced by this moment:

$$\frac{L}{\sqrt{2}} \frac{F}{4} = M \quad (A.10)$$

Combining Equations (A.9) and (A.10), we get the force generated by flexural stresses at the hinges:

$$F = 8 \left( \frac{t_B}{2} \right)^2 \sigma_B \quad (A.11)$$

Received: June 21, 2011  
Final Version: August 10, 2011

- [1] L. F. Wang, J. H. Song, C. Ortiz, M. C. Boyce, *J. Mater. Res.* **2009**, *24*, 3477.
- [2] F. G. Torres, O. P. Troncoso, J. Nakamatsu, C. J. Grande, C. M. Gomez, *Mat. Sci. Eng. C Bio. S* **2008**, *28*, 1276.
- [3] B. J. F. Bruet, J. H. Song, M. C. Boyce, C. Ortiz, *Nat. Mater.* **2008**, *7*, 748.
- [4] T. Ikoma, H. Kobayashi, J. Tanaka, D. Walsh, S. Mann, *Int. J. Biol. Macromol.* **2003**, *32*, 199.
- [5] T. Ikoma, H. Kobayashi, J. Tanaka, D. Walsh, S. Mann, *J. Struct. Biol.* **2003**, *142*, 327.
- [6] K. V. Kardong, *Vertebrates: Comparative Anatomy, Function, Evolution*, McGraw-Hill, New York **2008**.
- [7] L. Zylberberg, J. Geraudie, F. Meunier, J. Sire, *Bone* **1992**, *4*, 171.
- [8] J. Bereiter-Hahn, L. Zylberberg, *Comp. Biochem. Phys. A* **1993**, *105*, 625.
- [9] S. Sudo, K. Tsuyuki, Y. Ito, T. Ikohagi, *JSME Int. J. C Mech. Sy.* **2002**, *45*, 1100.
- [10] J. Y. Sire, *J. Fish Biol.* **1986**, *28*, 713.
- [11] J. D. Currey, *J. Exp. Biol.* **1999**, *202*, 3285.
- [12] J. H. Long, B. Adcock, R. G. Root, *Comp. Biochem. Physiol. A Mol. Integr. Physiol.* **2002**, *133*, 911.
- [13] J. H. Long, M. E. Hale, M. J. McHenry, F. M. W. Westneat, *J. Exp. Biol.* **1996**, *199*, 2139.
- [14] J. H. Long, T. J. Koob, K. Irving, K. Combie, V. Engel, N. Livingston, A. Lammert, J. Schumacher, *J. Exp. Biol.* **2006**, *209*, 4732.
- [15] M. R. Hebrank, J. H. Hebrank, *Biol. Bull.* **1986**, *171*, 236.
- [16] M. A. Meyers, A. Y. M. Lin, Y. Seki, P. Y. Chen, B. K. Kad, S. Bodde, *JOM J. Miner. Metals Mater. Soc.* **2006**, *58*, 35.
- [17] P. Fratzl, R. Weinkamer, *Prog. Mater. Sci.* **2007**, *52*, 1263.
- [18] L. J. Szewciw, D. G. de Kerckhove, G. W. Grime, D. S. Fudge, *P. Roy. Soc. B Biol. Sci.* **2010**, *277*, 2597.
- [19] F. J. Vernerey, F. Barthelat, *Int. J. Solids Struct.* **2010**, *47*, 2268.
- [20] M. R. Hebrank, *Biol. Bull.* **1980**, *158*, 58.
- [21] L. A. Jawad, *J. Nat. Hist.* **2005**, *39*, 2643.
- [22] W. T. Liu, Y. Zhang, G. Y. Li, Y. Q. Miao, X. H. Wu, *J. Fish Biol.* **2008**, *72*, 1055.
- [23] A. A. Schonborner, G. Boivin, C. A. Baud, *Cell Tissue Res.* **1979**, *202*, 203.
- [24] R. V. Seshaiya, P. Ambujabay, M. Kalyani, Amino acid composition of Ichthylepedin from fish scales, in: *Aspects of Protein Structure* (Ed: G. N. Ramachandran), Academic Press, New York p. 343.
- [25] F. J. Meunier, *Am. Zool.* **1984**, *24*, 953.
- [26] A. Bigi, M. Burghammer, R. Falconi, M. H. J. Koch, S. Panzavolta, C. Riekel, *J. Struct. Biol.* **2001**, *136*, 137.
- [27] L. Zylberberg, J. Bereiterhahn, J. Y. Sire, *Cell Tissue Res.* **1988**, *253*, 597.
- [28] F. J. Meunier, J. Castanet, *Zool. Scr.* **1982**, *11*, 141.
- [29] J. Meunier, *Tissue Cell* **1981**, *13*, 165.
- [30] T. M. Scheyer, P. M. Sander, W. G. Joyce, W. Boehme, U. Witzel, *Org. Divers Evol.* **2007**, *7*, 136.
- [31] E. C. Bass, F. A. Ashford, M. R. Segal, J. C. Lotz, *Ann. Biomed. Eng.* **2004**, *32*, 1231.
- [32] L. Zylberberg, J. Bonaventure, L. Cohensolal, D. J. Hartmann, J. Bereiterhahn, *J. Cell Sci.* **1992**, *103*, 273.
- [33] H. S. Youn, T. J. Shin, *J. Struct. Biol.* **2009**, *168*, 332.
- [34] F. J. Meunier, P. M. Brito, *Cybium* **2004**, *28*, 225.
- [35] C. Liu, S. Shen, *J. Taiwan Museum* **1991**, *44*, 321.
- [36] G. K. Ostrander, *The Laboratory Fish*, Academic Press, Oxford **2000**.
- [37] F. Barthelat, J. Poissant, *Exp. Mech.* **2010**, *50*, 353.
- [38] Z. L. Shen, M. R. Dodge, H. Kahn, R. Ballarini, S. J. Eppell, *Biophys. J.* **2008**, *95*, 3956.
- [39] K. J. Hartman, *Proc. Atlantic Striped Bass Workshop and Roundtable Discussion*, 1999, p. 6.
- [40] W. E. Bemis, A. Giuliano, B. McGuire, *Zoology* **2005**, *108*, 317.
- [41] H. Onozato, N. Watabe, *Cell Tissue Res.* **1979**, *201*, 409.
- [42] F. Barthelat, R. Rabiei, *J. Mech. Phys. Solids* **2011**, *59*, 829.
- [43] M. J. Buehler, *Nano Today* **2010**, *5*, 379.
- [44] S. Keten, Z. P. Xu, B. Ihle, M. J. Buehler, *Nat. Mater.* **2010**, *9*, 359.